

Supplementary Information

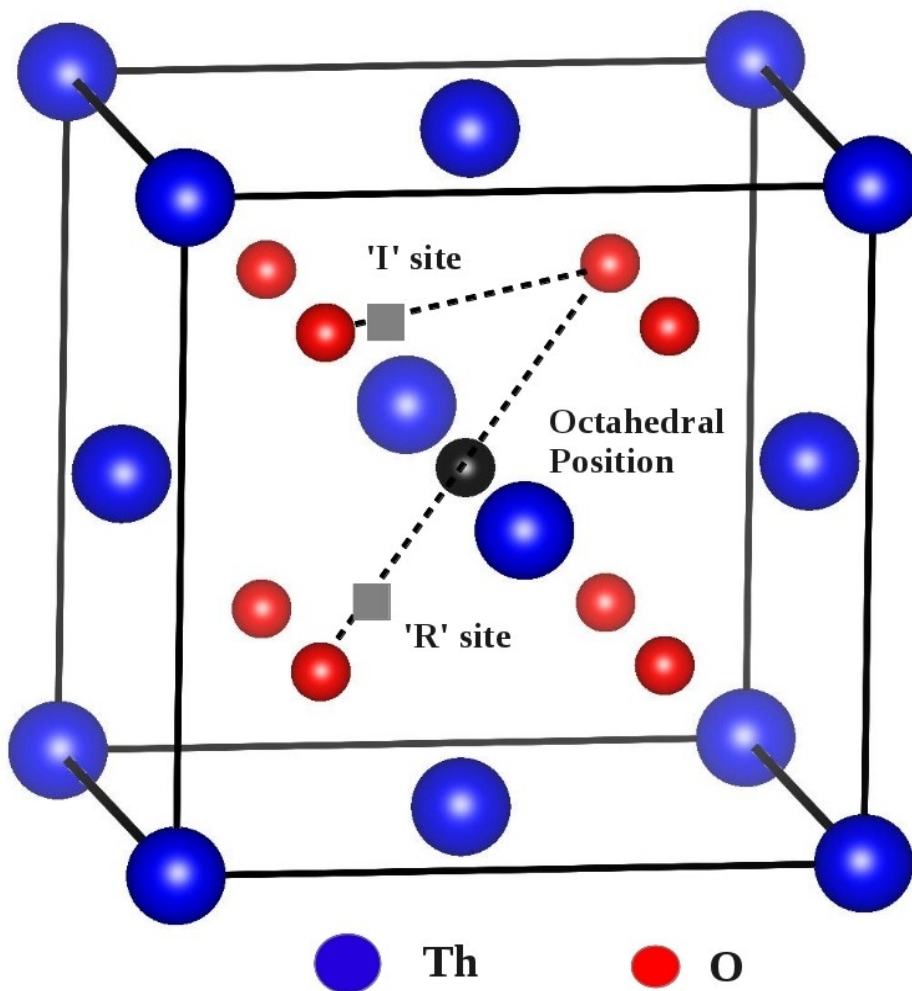


Figure SI-1: Illustration of ThO₂ fluorite unitcell containing 4 Th atoms located at (4a) Wyckoff positions (usual fcc positions) and 8 O atoms located at (8c) Wyckoff positions (tetrahedral positions). Octahedral position and other “I” and “R” interstitial positions are also shown.

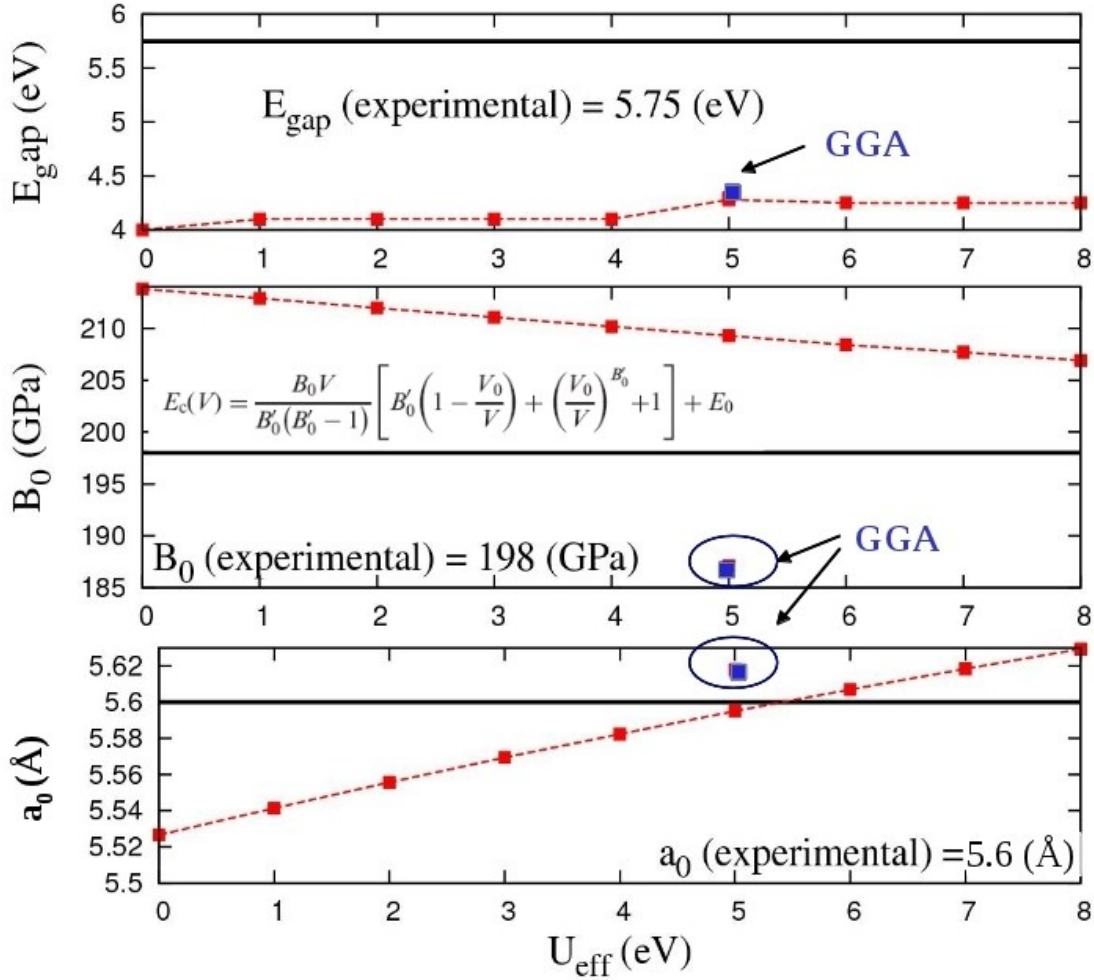


Figure SI-2: Variation of equilibrium lattice constant (a_0), bulk modulus (B_0) and electronic energy-gap (E_g) as a function of U_{eff} calculated for LDA+ U . Experimental values are presented as horizontal solid lines in the graph. This graph also shows GGA calculated values of a_0 , B_0 and E_g for comparison with LDA+ U calculated values. For the calculation of bulk modulus the Birch-Murnaghan equation of state was employed as shown in the B_0 vs. U_{eff} plot.

Table SI-1: LDA, LDA+U and GGA calculated equilibrium lattice constant (a_0), bulk modulus (B_0), equilibrium volume (V_0), pressure derivative of bulk modulus (dB_0/dP) and electronic energy-gap (E_g) for ThO₂.

| Methodology | a_0 (Å) | B_0 (GPa) | V_0 (Å ³) | dB/dP | E_g (eV) |
|----------------------------|-----------------------------------|---------------------------------|-------------------------|-------------------------------|------------|
| LDA | 5.5266 | 213.8 | 42.20 | 4.22 | 4.00 |
| LDA+U_{eff} | | | | | |
| U _{eff} = 1 | 5.5414 | 212.9 | 42.54 | 4.24 | 4.10 |
| U _{eff} = 2 | 5.5557 | 211.9 | 42.87 | 4.25 | 4.10 |
| U _{eff} = 3 | 5.5695 | 211.1 | 43.19 | 4.26 | 4.10 |
| U _{eff} = 4 | 5.5823 | 210.2 | 43.49 | 4.27 | 4.10 |
| U _{eff} = 5 | 5.5951 | 209.3 | 43.79 | 4.29 | 4.25 |
| U _{eff} = 6 | 5.6070 | 208.4 | 44.07 | 4.30 | 4.25 |
| U _{eff} = 7 | 5.6185 | 207.7 | 44.34 | 4.31 | 4.25 |
| U _{eff} = 8 | 5.6294 | 206.9 | 44.60 | 4.33 | 4.25 |
| GGA | 5.619 | 187.4 | 44.33 | 4.23 | 4.30 |
| Experiment | (5.598(4)) [1] (5.6001(3)) [2] | (195.3±2.0) [1] (198(2)) [2] | | (5.4±0.2) [1] (4.6(3)) [2] | 5.75 [3] |

[1] J. Staun Olsen, L. Gerward, V. Kanchana, G. Vaitheeswaran, Journal of Alloys and Compounds 381 (2004) 37–40.

[2] M. Idiri, T. Le Bihan, S. Heathman, J. Rebizant, Phys. Rev. B 70 (2004) 014113.

[3] E. T. Rodine and P. L. Land, Phys. Rev. B 4 (1971) 2701.

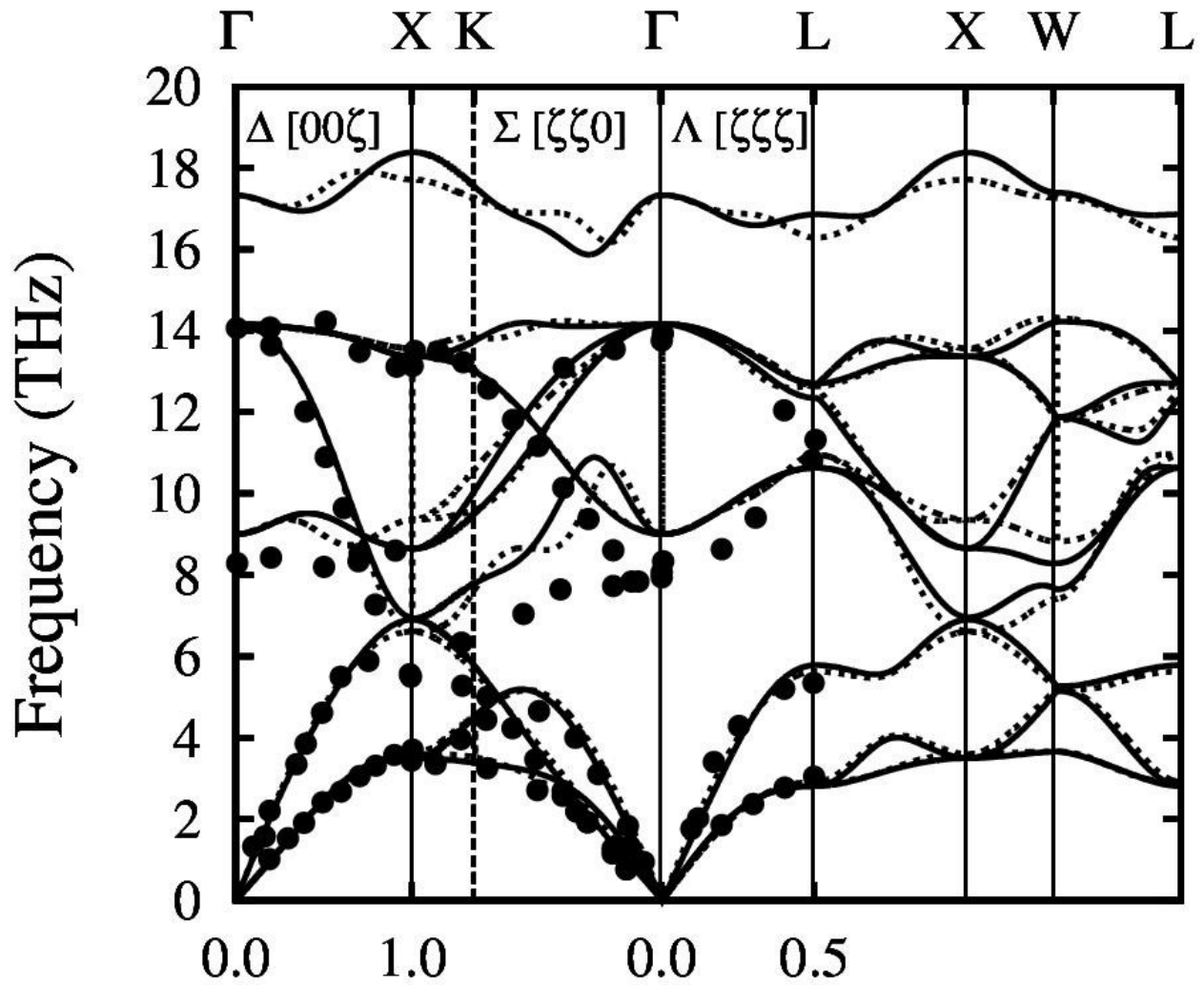


Figure SI-3: Phonon dispersion curves for ThO₂ calculated using LDA+U and 3x3x3 supercell (81 atoms) and a 4x4x4 supercell (192 atoms), compared with inelastic neutron scattering data at room temperature. The solid and dotted lines represents calculated phonon frequencies for the 3x3x3 and 4x4x4 supercell, respectively. Solid points are neutron scattering data as reported by Clausen *et al.* [46].

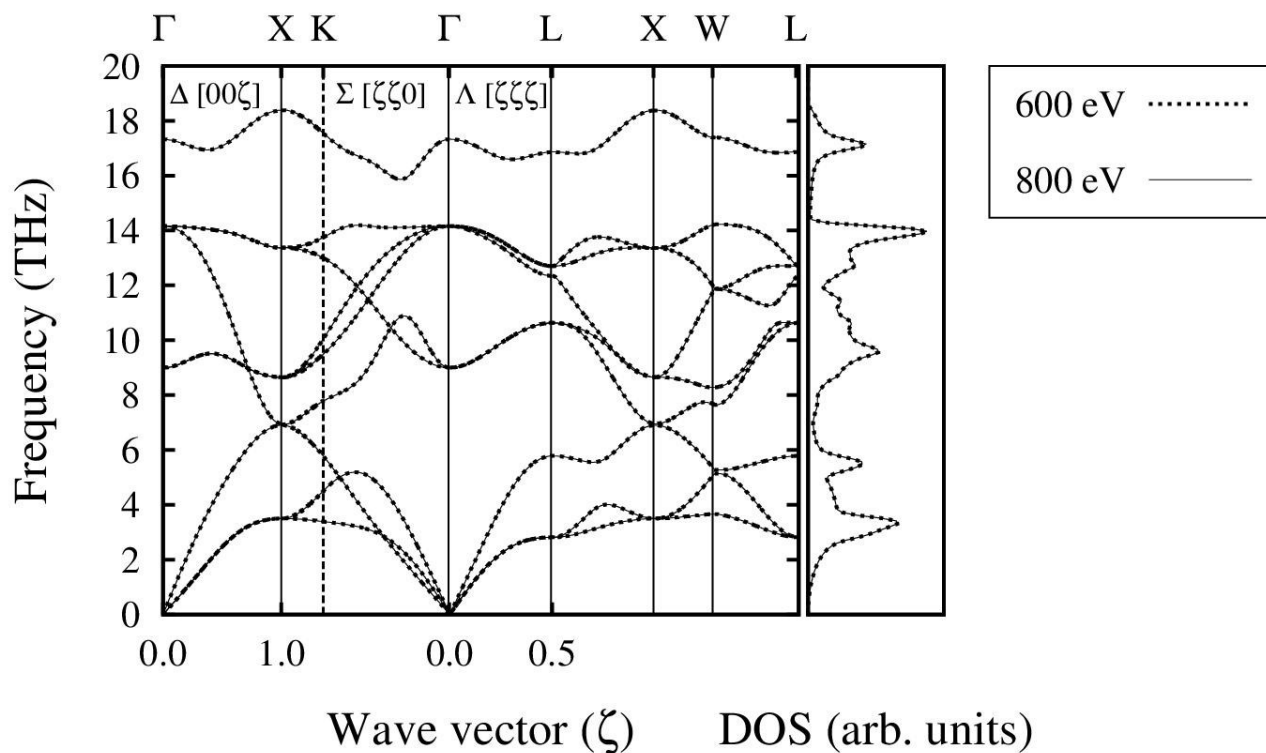


Figure SI-4: Phonon dispersion curve and phonon density of states of ThO₂ calculated using LDA+*U* ($U_{\text{eff}} = 5$ eV), 3x3x3 (81 atoms) supercell, 8x8x8 k-point mesh compared for ENCUT = 600 eV and 800 eV. The lack of difference in phonon dispersion curve and phonon DOS is consistent with convergence of phonon dispersion calculations with respect to the value of ENCUT.

We have calculated phonon dispersion curve of ThO₂ using LDA+*U* ($U_{\text{eff}} = 5$ eV), 3x3x3 supercell (81 atoms), 8x8x8 k-point mesh with E_{cutoff} of 600 eV (already given in the manuscript). We checked for E_{cutoff} convergence by raising E_{cutoff} to 800 eV. The figure given below compares phonon dispersion curve and phonon DOS calculated using E_{cutoff} s of 600 eV and 800 eV. There is no change in the phonon frequencies and phonon DOS in going from 600 eV to 800 eV which shows that our calculations are converged with E_{cutoff} parameter.

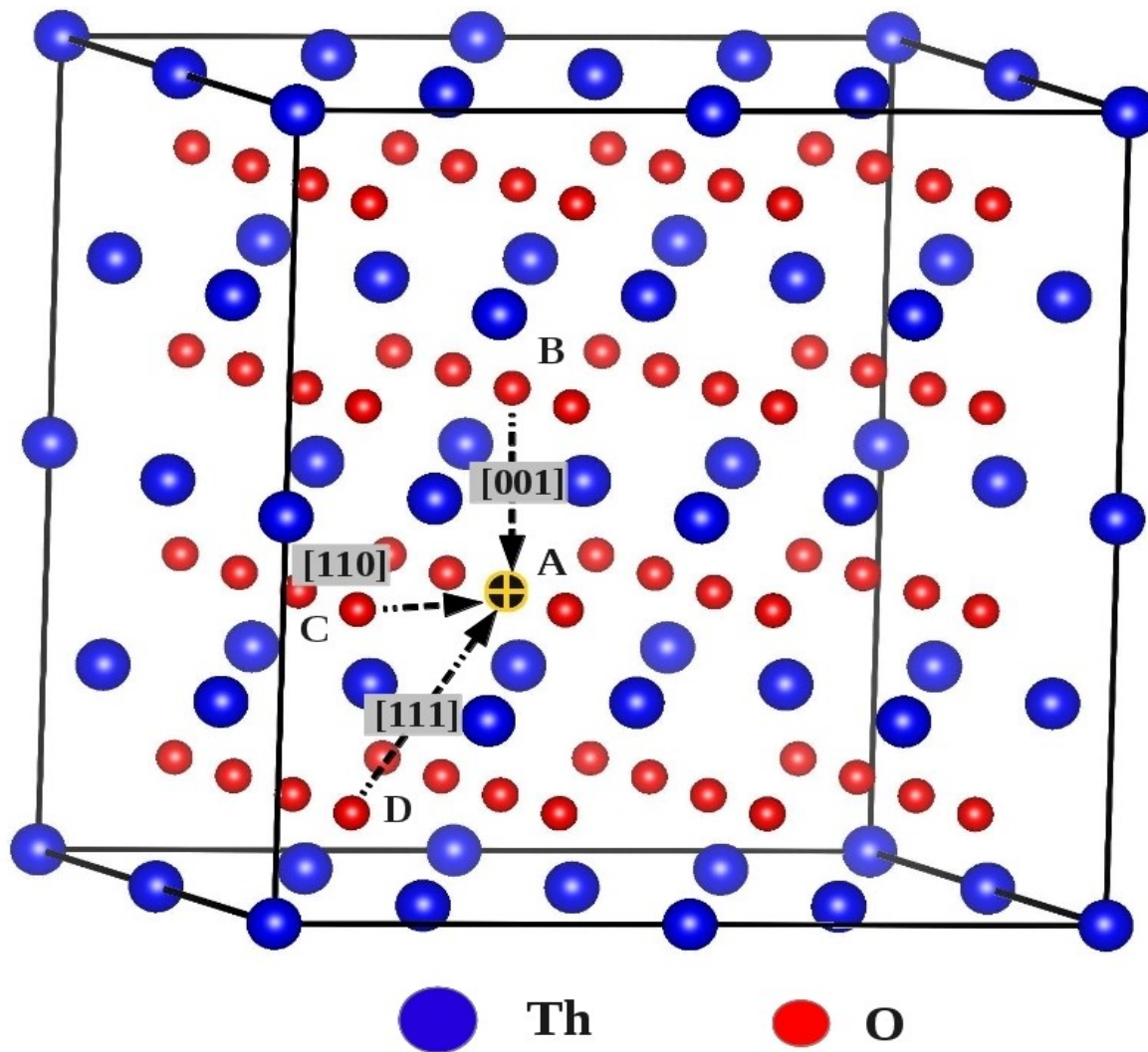


Figure SI-5: Illustration of oxygen migration directions towards a vacant oxygen site A (black atom) in a 2x2x2 supercell (96 atoms). Atoms B, C and D migrate to position A along [001], [110] and [111] directions, respectively. This supercell is taken only to show 3 migration direction and actual calculation was performed in a 10x10x10 supercell (12000 atoms).

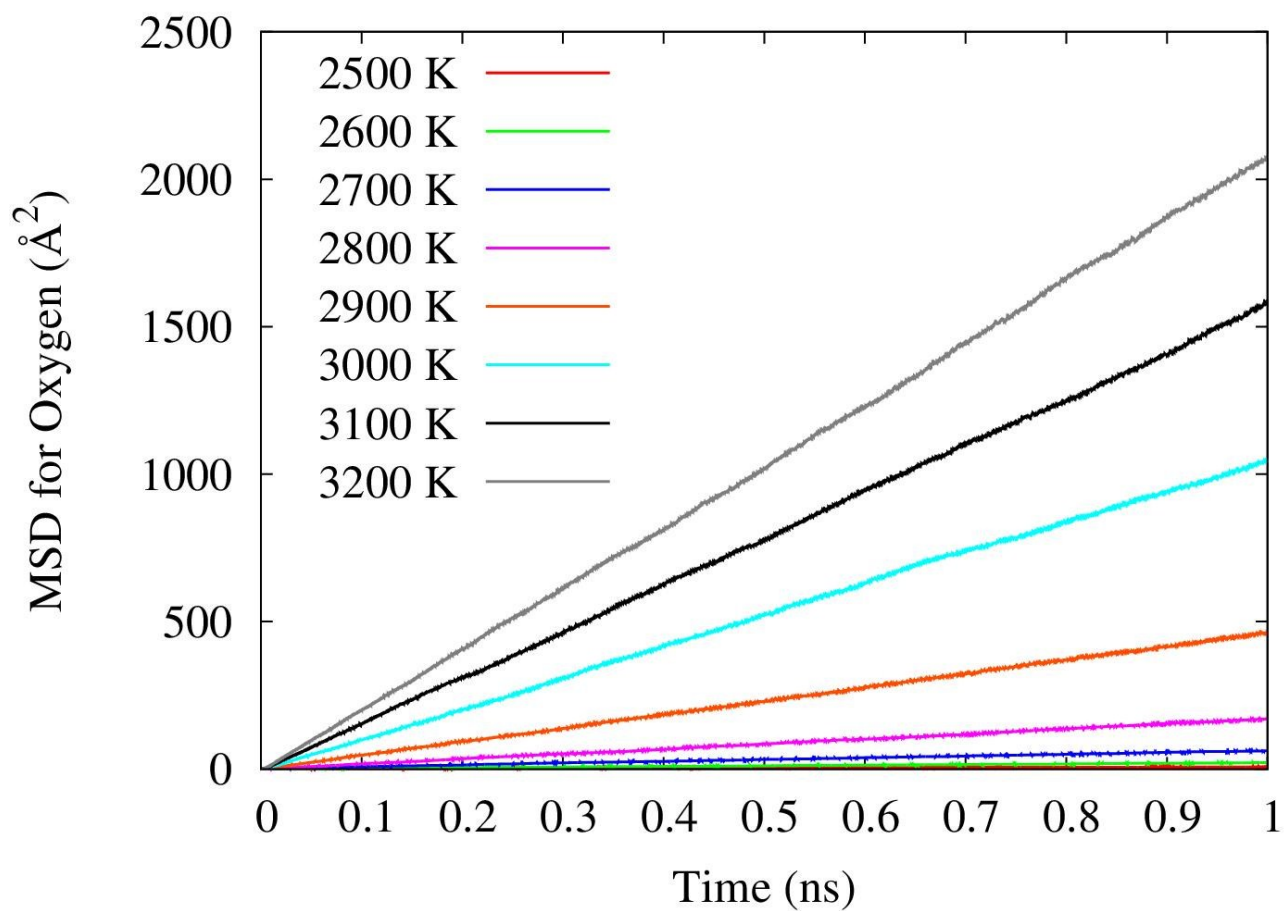


Figure SI-6: MD calculated MSD curve for oxygen between 2500 K and 3200 K (100 K interval). The superionic transition is visible above 2900 K.

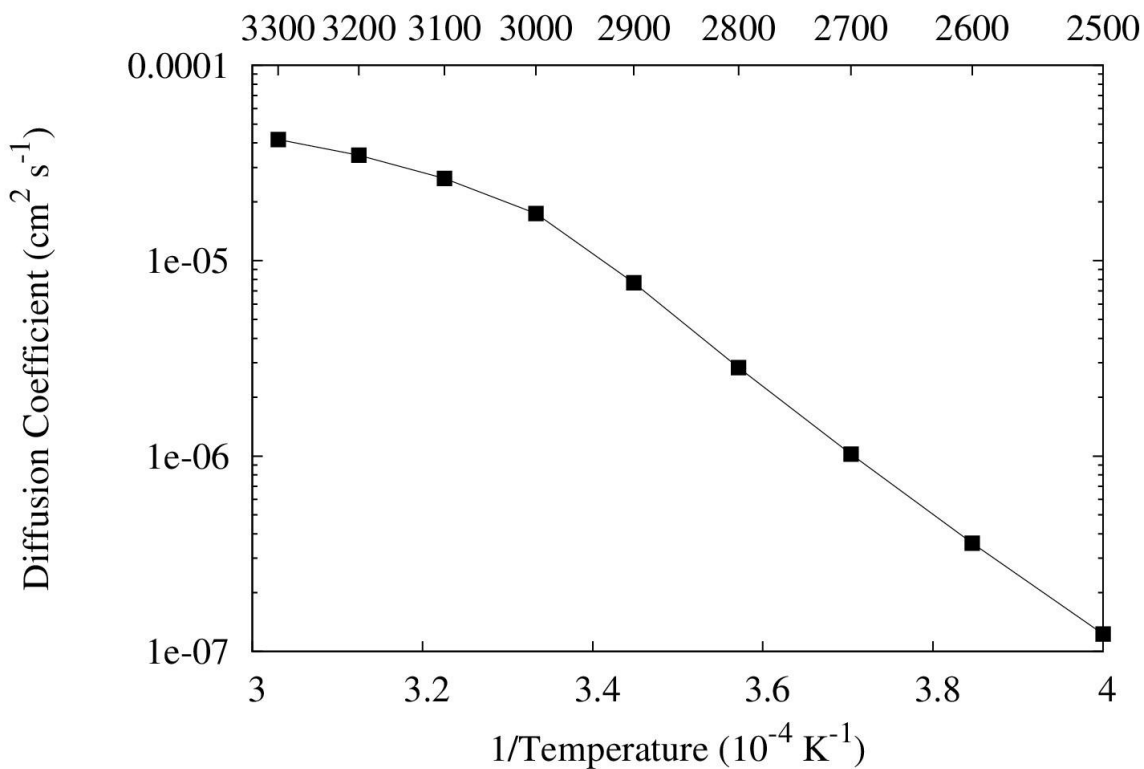


Figure SI-7: MD calculated diffusivity plot for oxygen between 2500 K and 3300 K (100 K interval). The jump in the diffusivity value appears at 3000 K and above.

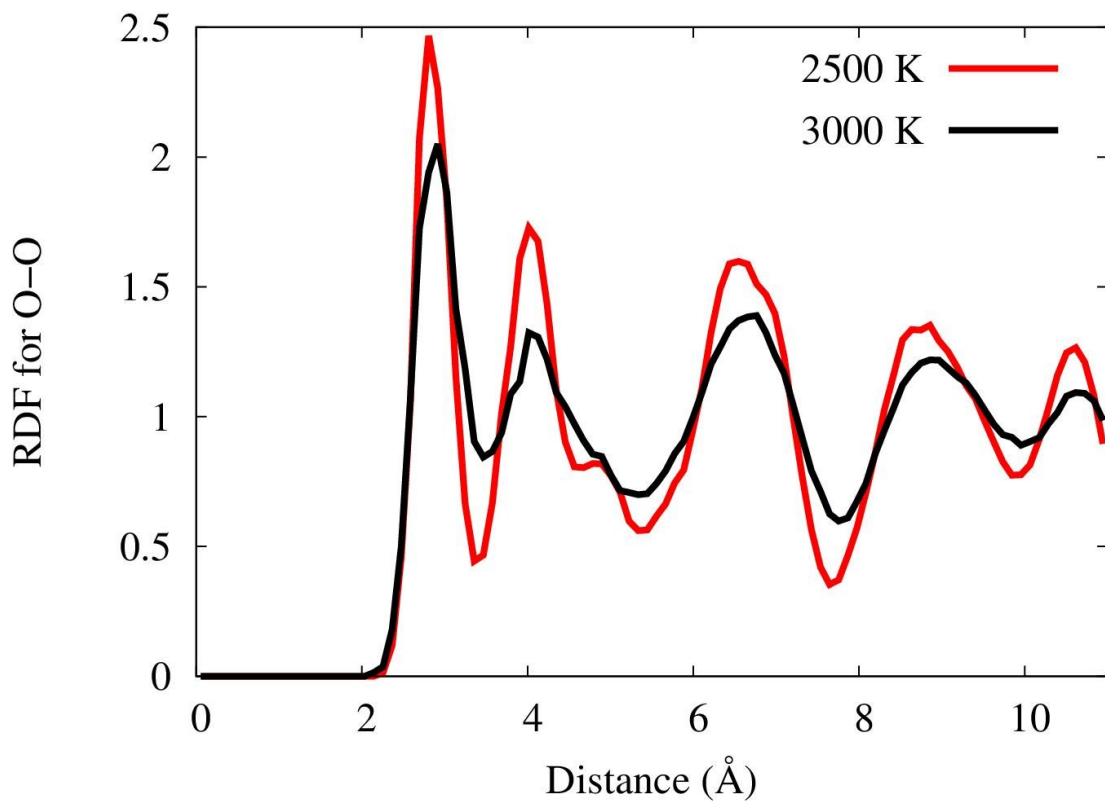


Figure SI-8: MD calculated O-O pair RDF plot at 2500 K and 3000 K. Below the fast ionic regime, simulated at 2500 K, the RDF shows a succession of well-defined peaks, while in the fast ionic regime the RDF peaks are less-well defined from 2nd nearest neighbours onwards. This indicates a more diffuse O sub-lattice because of intensive ionic motion.

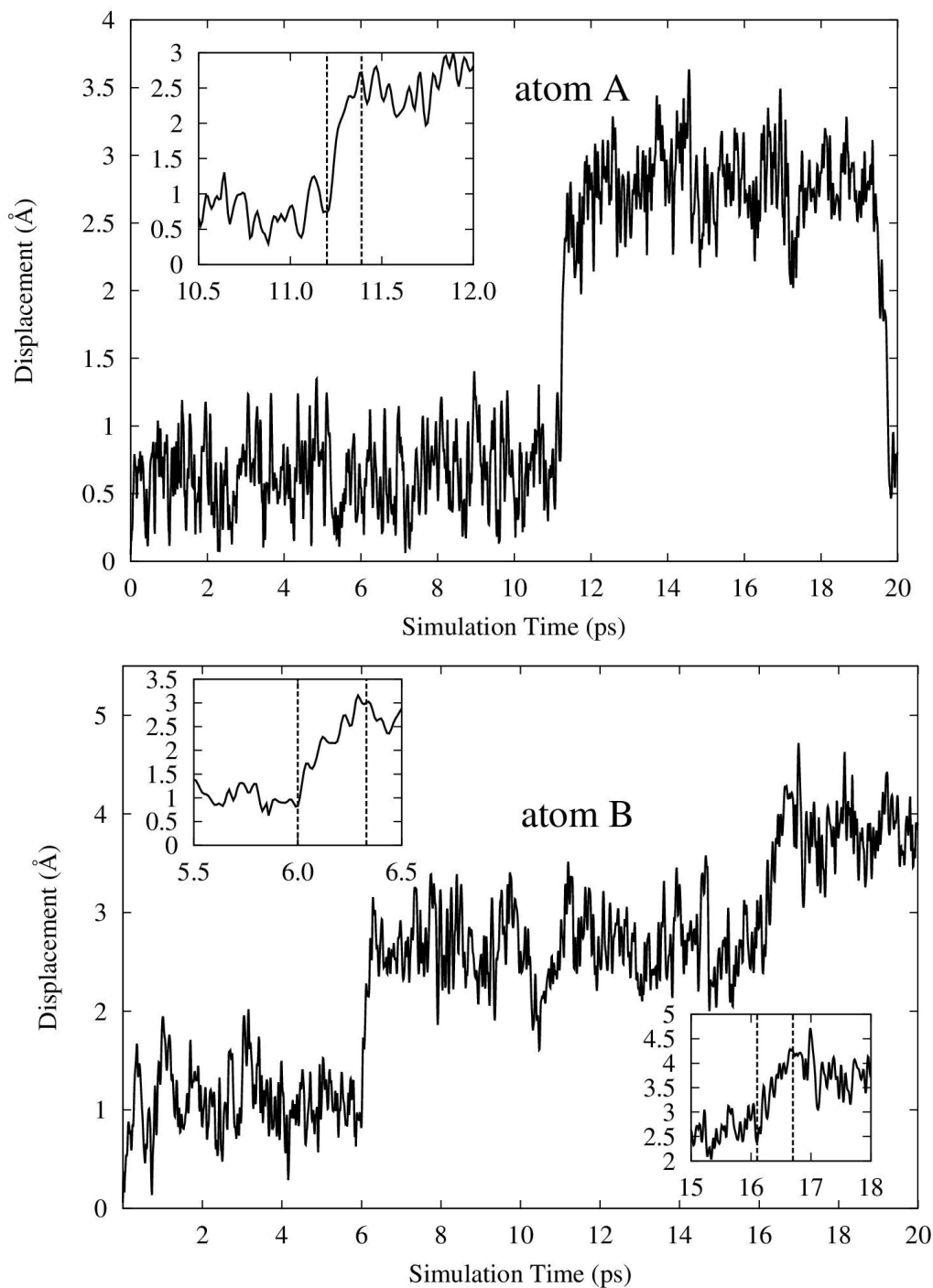


Figure SI-9: MD calculated total displacement ($\sqrt{(dx^2+dy^2+dz^2)}$) from equilibrium position is plotted as a function of simulation time for atom A (upper panel) and atom B (lower panel) at 3000 K temperature. Inset figures show simulation time corresponding to which anionic transition occurs from one tetrahedral position to the other.

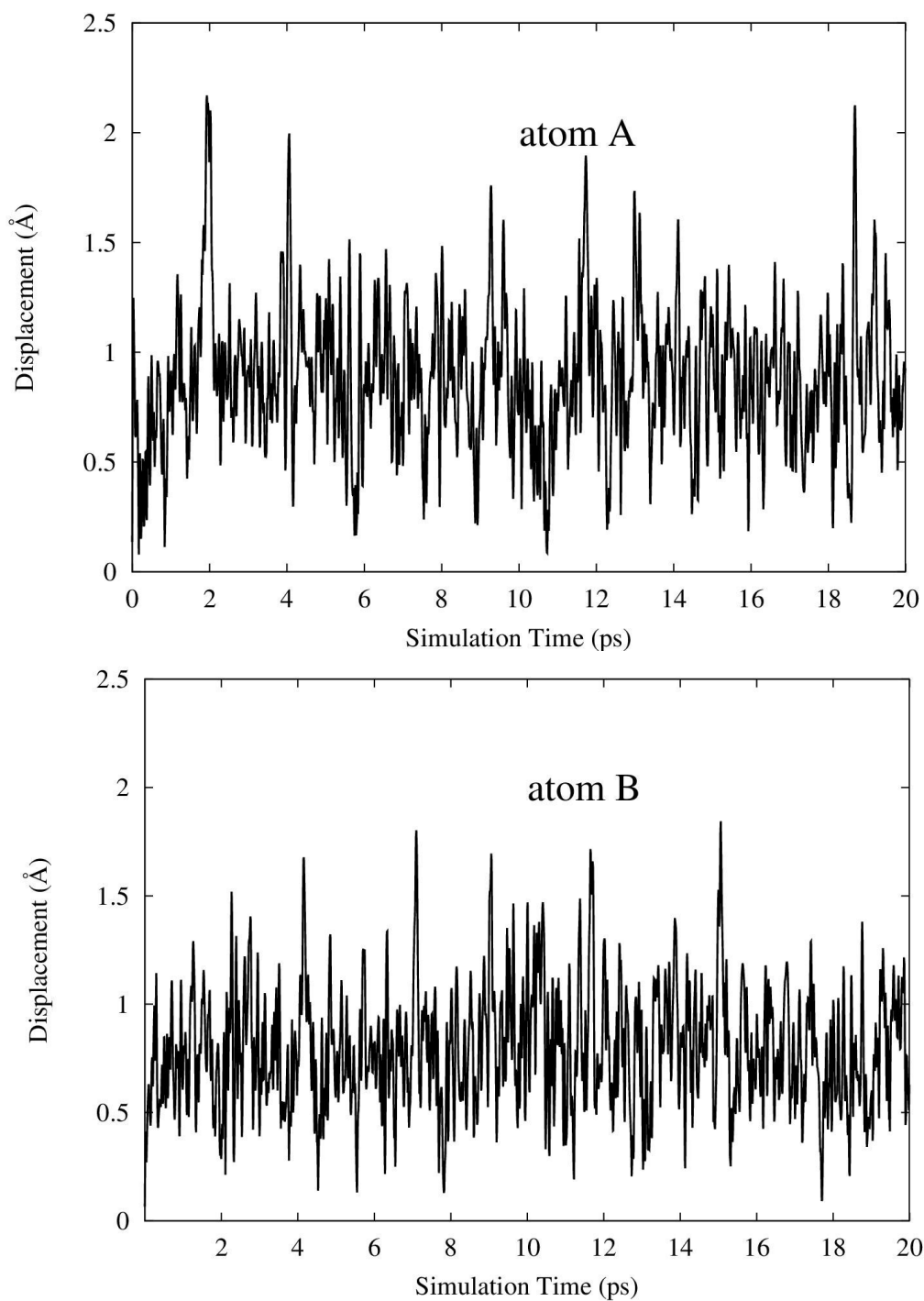


Figure SI-10: MD calculated total displacement ($\sqrt{dx^2+dy^2+dz^2}$) from equilibrium position is plotted as a function of simulation time for atom A (upper panel) and atom B (lower panel) at 2900 K temperature. Figures clearly show no anionic diffusive jumps from one tetrahedral position to the other.

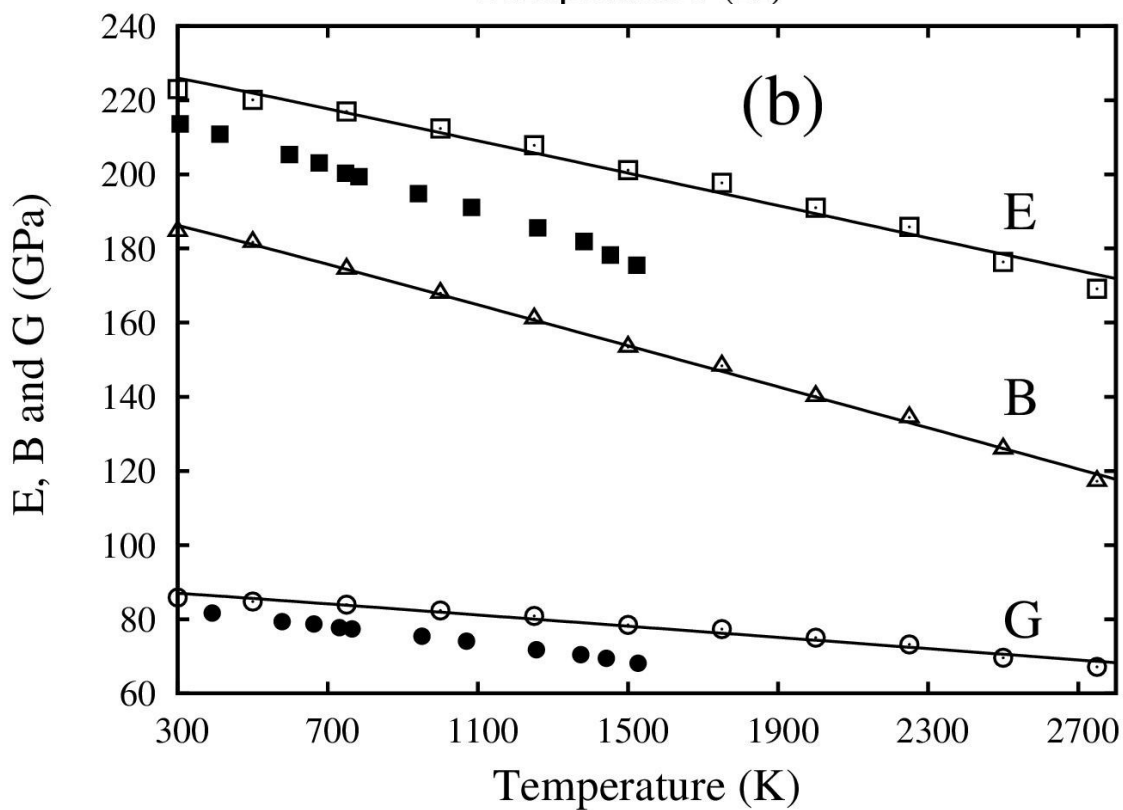
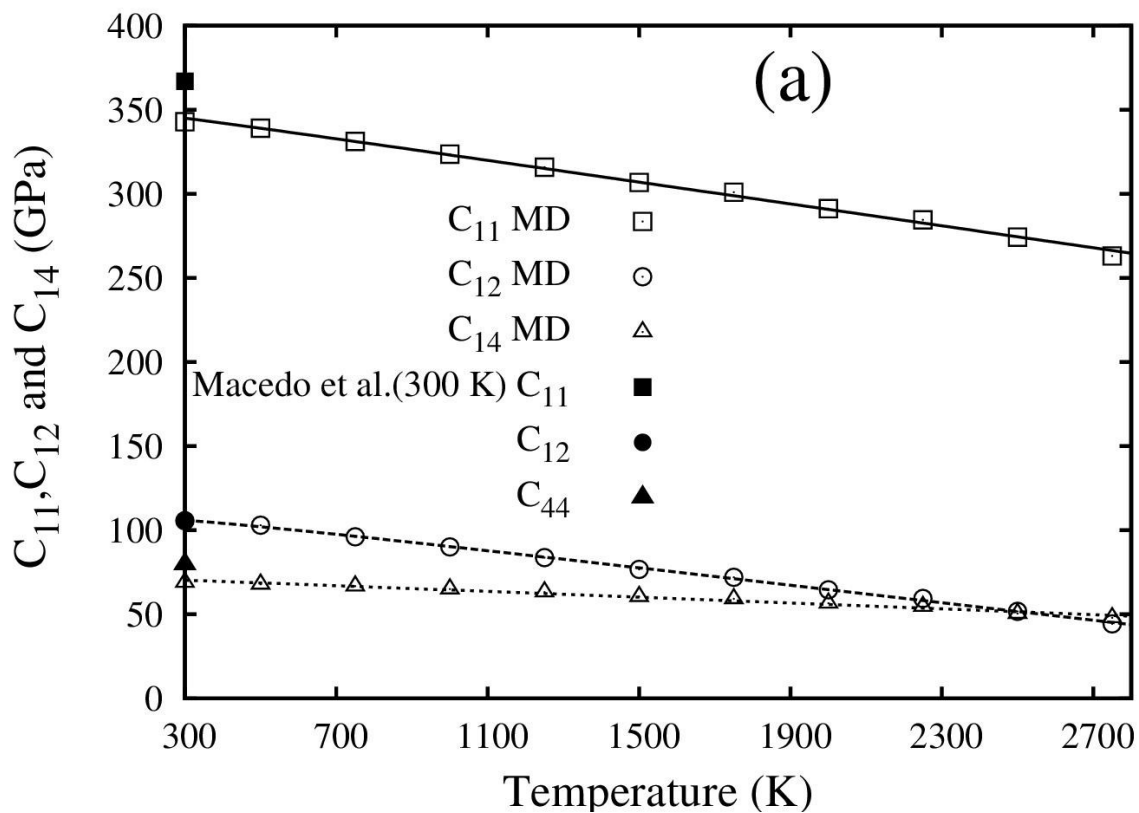


Figure SI-11: (a) MD calculated single crystal elastic constants (C_{11} , C_{12} and C_{44}) are shown as a function of lattice strain (temperatures). Experimentally measured room temperature values are also shown (measured by Macedo et al. [40] from single crystal ThO_2). **(b)** E , B and G values from MD calculated C_{11} , C_{12} and C_{44} values of ThO_2 as a function of temperature in the 300-2800 K range along with previous dynamic resonance measurements by Spinner *et al.* [SI1].

Fig. SI-11 presents our calculated E , B and G values from MD calculated C_{11} , C_{12} and C_{44} values of ThO_2 as a function of temperature in the 300-2800 K range, along with previous dynamic resonance measurements by Spinner *et al.* [SI1] for 6.95% porosity and 298-1523 K temperature range. **Fig. SI-11** highlights that MD calculated E and G values overestimate experimentally determined values over the whole temperature range and that the deviation from experimentally reported values are greater in the high temperature region. MD calculated values are fitted to polynomial equations in the temperature range of 300-2800 K, as given by;

$$E(T)/E(300) = 1.01961 - 0.08611 \times 10^{-4} T \exp(-181/T) \quad (1)$$

$$G(T)/G(300) = 1.01750 - 0.07536 \times 10^{-4} T \exp(-181/T). \quad (2)$$

Similarly, the polynomial fit to experimentally determined values in the 298-1300 K temperature range are given by Wolfe *et al.* [SI2]

$$E(T,p)/E(298,p) = 1.023 - 1.405 \times 10^{-4} T \exp(-181/T) \quad (3)$$

where $E(T,p)$ and $E(298,p)$ represents Young modulus at any temperature T with porosity content p and Young modulus at 298 K with porosity content p , respectively. The G values also follow the same temperature variation equation as E according to Wolfe *et al.* [SI2]. A comparison of the equations above shows that ThO_2 interatomic potentials are able to capture the coefficient of the $1/T$ term in the exponential and initial constant term correctly. But the underestimation of the coefficient of the exponential term changes the slope of the E vs. T line causing deviation from experimentally reported values. It is also important to note that, porosity has its major effect on E and G values but other microstructural features such as, pore size, pore distribution, grain size and inhomogeneity are also closely associated with the porosity factor. All these factors cumulatively affect E and G values at ambient as well as at high temperatures and in the present study it is difficult to analyze the extent of the effect of each factor independently. The deviation of the MD calculated values from the previous dynamical resonance measurements can be ascribed to these effects.

[SI1] S. Spinner, F.P. Knudsen and L. Stone "Elastic Constant-Porosity Relations for Polycrystalline Thoria" Journal of Research of the National Bureau of Standards C - Engineering and Instrumentation 67 (1963) 39-46.

[SI2] R.A. Wolfe and S.F. Kaufman, "Mechanical Properties of Oxide Fuels", WAPD-TM 587 (1967).